A passive low-frequency seismic survey in Abu Dhabi – Shaheen project

Birkelo, B., M. Duclos, B. Artman, B. Schechinger, B. Witten, A. Goertz, K. Weemstra, Spectraseis AG, and M.T. Hadidi, ADCO*

Summary

We present processing methods and results from a passive low-frequency (LF) seismic campaign over a giant producing oil field in Abu Dhabi. Processing methods include ambient wave field analysis and the mitigation of the influence of anthropogenic infrastructure noise. Without careful processing to remove these components of the ambient wave field, data are strictly measures of human activity. However, spatially and temporally consistent energy anomalies on the vertical component cluster within the center of the survey area. Available current reservoir data show some correlation with the energy attributes calculated with two different methods.

Introduction

Ambient wave field measurements over oil and gas fields have documented energy anomalies typically at frequencies between 1-6 Hz (Dangel, et al., 2003, Saenger et al., 2009). The Shaheen project was designed to record data over a giant producing oil field in Abu Dhabi to determine: 1) if this anomaly was present, 2) the spatial distribution of this anomaly, 3) the distribution of cultural noise that might impact the measurement of this anomaly, and 4) the correlation, if any, of this anomaly to the reservoir fluid system.

The underlying assumption with passive LF seismic recording is that data is the superposition of surface waves and relatively weak, body waves from depth that have been produced or modified by the hydrocarbon reservoir (hydrocarbon microtremor). The hydrocarbon microtremor is assumed to be quasi-stationary, while the surface-wave noise can vary significantly with time. We describe the work done to identify, understand and map the many sources of seismic noise present in this oil field.

Recent studies of passive seismic data in Abu Dhabi analyzing spectra of long, unedited time-window averages found only traffic-related surface waves in the ambient wave field above 1 Hz (Ali et al., 2010). The key to successfully mapping a hydrocarbon microtremor signal is to analyze quiet time windows where surface waves do not mask any weaker signal. We present the strategy used to separate the hydrocarbon microtremor signal from surface wave noise and the results from the data analysis. We then show a comparison of the final processed data to one measure of the fluid system of the oil and gas reservoirs.

Acquisition summary

Figure 1 shows a map of the Shaheen survey, acquired in February 2009. Red dots show eight lines of three-component broadband seismometers. Each line in the grid recorded for a minimum of 24 hours. Blue dots denote a 49-station six-arm array used to characterize the ambient wave field.

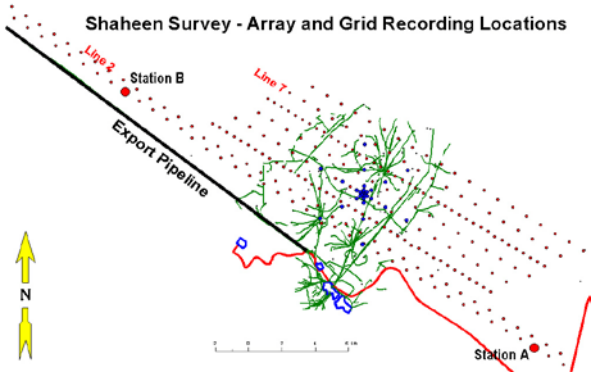

Figure 1: Shaheen grid (red dots) and array (blue dots) along with partial field infrastructure. The locations of stations A and B shown in Figure 5 are highlighted. Station A had strong traffic-generated noise while station B had strong continuous noise from the export pipeline. Lines 2 and 7 are labeled for later reference.

Ambient wave field

Characterizing the ambient wave field defined the processing strategy necessary to mitigate the surface noise obscuring the potential hydrocarbon microtremor. The red lines in Figure 1 are service roads and a highway. These introduce major surface wave noise that must be removed or avoided. Other oil field facilities affecting the ambient wave field include the oil pipeline system, the peripheral injection system, and central processing facilities (gray lines), as well as the main oil export pipeline. The oil export pipeline impacted the data severely, particularly in the NW of the survey.

Two types of noise sources are dominant in the data: (i) transient broadband noise related to road traffic that added up to 30 dB of energy in the 2-4 Hz range when present, and (ii) stationary noise from oilfield facilities. Figure 2 shows a spectrogram section for 20 stations from one of the survey lines. The two noise types transition smoothly along the line. Traffic transients originating from the highway

A passive low-frequency seismic survey in Abu Dhabi

East of the line (bottom) are identifiable across the whole line (20 km).

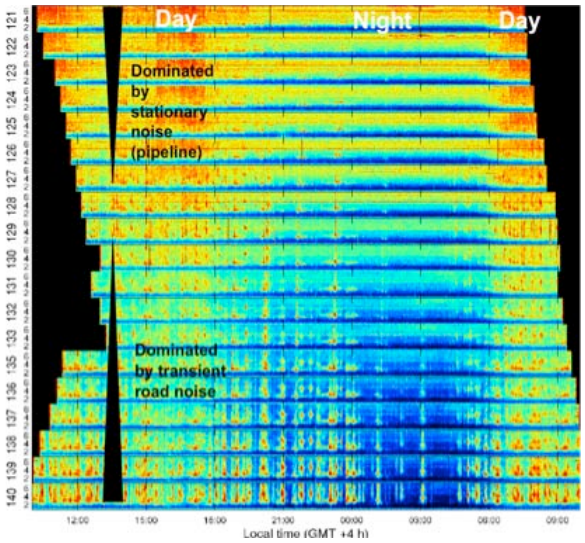

Figure 2: Spectrogram section of Z component for one of the 1 km-spaced seismometer lines indicated by red dots in Figure 1. The bottom of the section is closest to the highway. Each spectrogram shows frequencies between 0-10 Hz.

The 49-station array had variable station spacing along the spokes, ranging from 6 m in the center to 1500 m on the periphery in order to capture a wide range of apparent velocities. For beamforming analysis, the five days of data from the array were segmented into 20 s windows, with an overlap of 10 s. Pre-processing included automatic muting of transient events above a threshold defined by the ratio of the short/long time average of each trace. This processing scheme discards transient events and focuses on quasi-stationary arrivals.

Figure 3 shows representative results from the large volume of array data. The left panel shows near zero wave-number energy. Side lobes are due to the geometric array transfer function. No significant events in the global seismicity catalogues were expected to arrive during this time interval. The right panel is an example that is much more common in the total volume of data. The radius of the beam focus corresponds to a velocity of ~700 m/s, and the azimuth is from the SW. This is consistent with surface waves emanating from the field infrastructure to the SW.

Dispersion analysis

Azimuthal summation of the single frequency beams (Figure 3) builds a slowness vs. frequency space, commonly used to identify dispersive wave modes. Figure 4 shows the velocity vs. frequency energy histogram from a 2 hour window. This dispersion curve can be inverted for the shear wave velocity profile underneath the array, The black line shows the fundamental-mode Rayleigh wave as forward-modelled from an inverted velocity profile. The dashed circle highlights a narrow-banded non-dispersive body-wave mode that stretches over a range of high phase velocities. The very strong energy between the fundamental-mode Rayleigh wave and the body wave is a mix of the next higher Rayleigh mode and the fundamental-mode Love wave. The dispersion curve shows that most of the energy is in the fundamental- or higher-mode surface waves. Nevertheless, body wave arrivals are distinguishable.

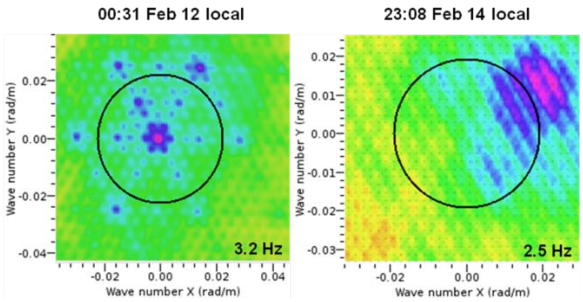

Figure 3: 20 s window beam energy. Circles at 700 m/s velocity. Left: body wave arrival at 3.2 Hz, right: surface wave arrival from the SW at 2.5 Hz.

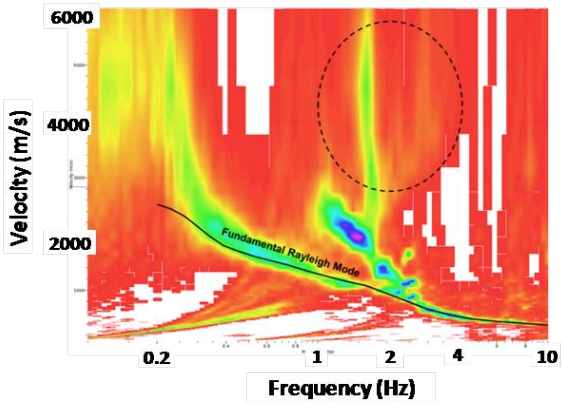

Figure 4: Velocity-frequency energy histogram from the array data showing surface and body wave energy.

Data processing

To mitigate the effect of surface waves, we apply a processing sequence of time editing, calculation of frequency-domain attributes, and waveform back-propagation. Identifying time windows where human activity and infrastructure noise is reduced is essential. The quietest time for this survey was 3-5 am local time. A frequency-domain attribute, PSD-IZ, was calculated by integration of the vertical-component power spectrum in a selected frequency band (Saenger et al., 2009, Lambert et al., 2009). Waveform back-propagation uses the elastic wave equation to locate sources of body wave energy and separates surface waves from body waves in the depth domain.

Spectrograms provide a means to characterize the ambient wave field and to identify transient events for removal. The

A passive low-frequency seismic survey in Abu Dhabi

top two panels of Figure 5 show a spectrogram of station A near a highway before and after transient removal. The right columns are histograms of the data where warm colours indicate a large number of occurrences of a spectral level over the investigated time interval. The upper histogram shows a bimodal distribution related to traffic / no traffic states. If a long time window average of unedited data is used (Ali et al., 2010), the spectra will only reflect the higher mode (upper panel, Figure 5a). Editing of transients reduces the variability, allowing the average spectral to track the lower bound of the distribution, representative of the natural background wave field at this location (lower panel, Figure 5a). The bottom row (Figure 5b) shows a spectrogram from Station B near the export pipeline in the NW of Figure 1 that is dominated by stationary noise. Time editing hardly affects this type of data and does not alter its average.

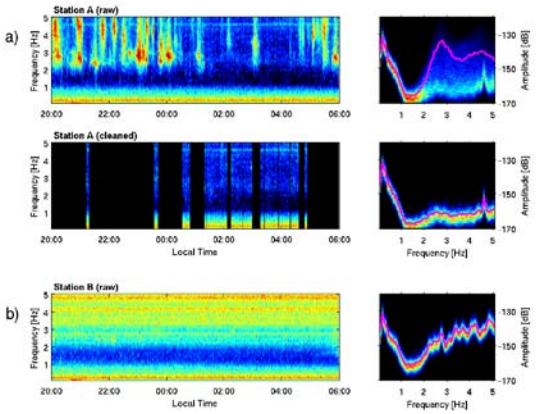

Figure 5: Cleaning transient traffic noise from data by muting time windows. Mean spectrum (magenta curve) is reduced to the background. b) Continuous pipeline noise that can not be removed by muting time windows.

Back-propagation of the waveform data into the depth-domain allows separating the surface waves from body waves. Time-reverse imaging (TRI) combines back-propagation of the wave field (Saenger, 2000), application of elastic imaging conditions (Artman et al. 2009), and normalization of the data for acquisition artifacts and lateral variations of noise levels (Witten and Artman, 2010). Due to their evanescent nature, surface waves remain in the shallow part of the image when back-propagated, whereas body wave components with near-vertical incidence angles travel to greater depths in the image. We quantify the body waves by image-domain energy attributes (TRI-E) representing the average energy per normalized depth trace, excluding the upper 500 m of the image. The TRI-E attributes are similar to the PSD-IZ attributes in the quieter areas, but are much less affected by the surface waves in the noisy areas because of the partial body-wave mode separation due to wave field propagation in depth.

Figure 6 shows a comparison between PSD-IZ, TRI-E, and a noise proxy along with reservoir data from the field for Line 7, in a quieter area of the field. The noise proxy is the PSD integral from 5-10 Hz, where oil field facility noise is abundant. Columns indicate the cumulative hydrocarbon column in relative values, estimated for the time of the survey. Figure 7 shows the same comparison for Line 2, located near the oil export pipeline.

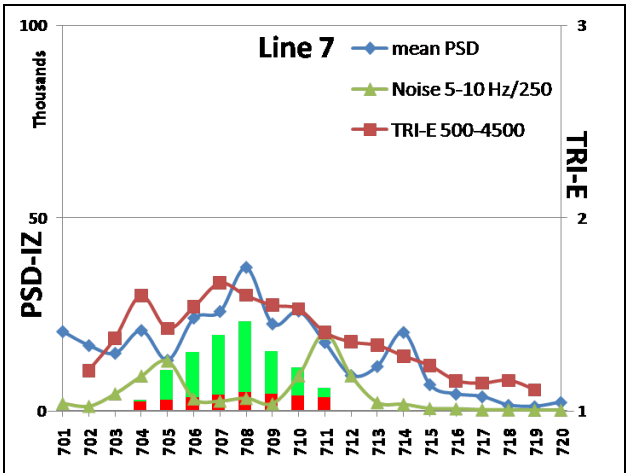

Figure 6: PSD-IZ, TRI, noise, and relative cumulative hydrocarbon column comparisons for Line 7. Maximum for PSD-IZ, TRI-E and hydrocarbon thickness coincide. Noise maixima are at the edges of the field. Oil (green) and gas (red) thickness are relative

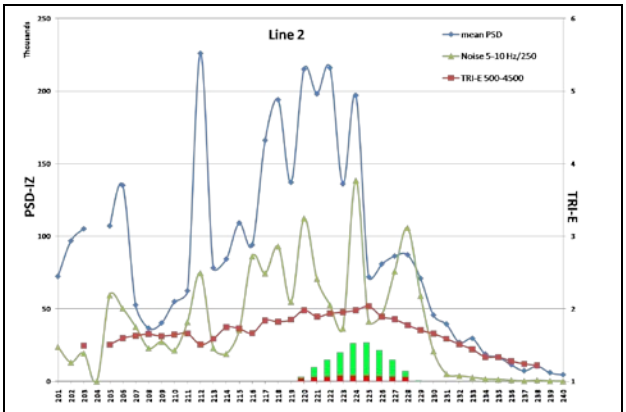

Figure 7: PSD-IZ, TRI, noise, and relative cumulative hydrocarbon column comparisons for Line 2. Lateral distance is twice that of Line 7 in figure 6. Vertical scale is 2.5 times that of Line 7. All data is scaled vertically in proportion to figure 6.

For Line 7 (Figure 6), both PSD-IZ and TRI-E attributes reach their maximum over the thickest accumulation hydrocarbons at stations 707 and 708. The strongest noise on Line 7 occurs at the edge of the field at stations 705 and 711. In contrast, along relatively noisy Line 2 (Figure 7), PSD-IZ values are correlated to the pipeline noise. TRI-E values reach their maximum over the thickest hydrocarbons and are less sensitive to the noise from infrastructure. Some noise is still influencing the TRI-E calculation though, evidenced by the TRI-E values remaining above 1.5 rather than dropping back to the no-signal value of one (Witten and Artman, 2010). On all profiles and maps, low attribute values persist on the east side of the survey, corresponding to areas off the reservoir. This area provides an estimate of the energy level of the ambient wave field free of traffic

A passive low-frequency seismic survey in Abu Dhabi

noise and potential hydrocarbon microtremors. In addition to attributes derived from ambient noise measurements, we also observe increased PSD-IZ values after an M6.9 earthquake during the passage of the VLF (< 0.1 Hz) surface wave train of the earthquake. This increase is only observed on stations above the thickest hydrocarbon column (Figure 8).

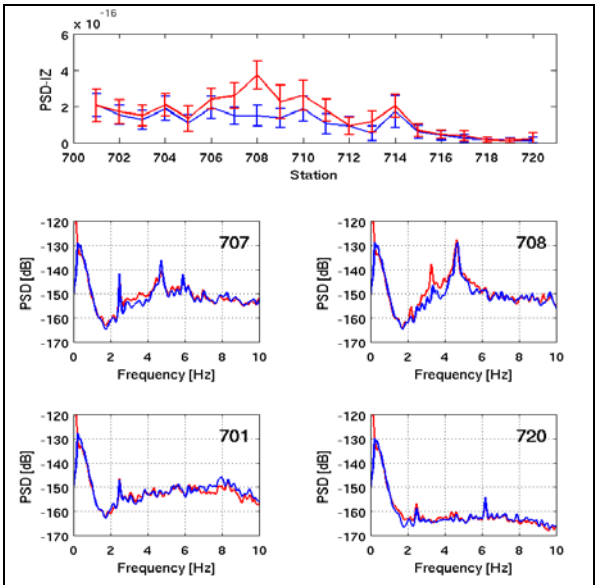

Figure 8: PSD-IZ profiles and station spectra from Line 7 recorded during the surface wave train of a M6.9 teleseismic earthquake (red curves). Stations over the reservoir, 707 and 708, show increased PSD-IZ between 2-6 Hz during this period compared to the previous night (blue curves).

Figure 9 shows cross plots of TRI-E attributes and net hydrocarbon column for all lines, specifically highlighting Lines 2 and 7. The overall R^2 for the eight lines taken together is lower than the individual lines separately. Nevertheless, approximately parallel trends, albeit offset from each other, are observed for lines in the survey relating the ambient wave field energy and the reservoir hydrocarbon column. The offset is a noise effect due to the propagation filter not removing the stationary pipeline noise completely. Further improvement of the results of this survey hinges on the ability to further mitigate the pipeline noise.

Conclusions

Body waves are present in the ambient wave field over a giant oil field in Abu Dhabi. With methods based on beam forming, we found high apparent velocity energy within the ambient wave field, even under the restriction of only analyzing the single most energetic beam over short time windows. Seismic energy with such high apparent velocity may carry information about the deeper subsurface.

With an understanding of the surface noise present in the area, we designed a data processing strategy to limit the impact of surface noise on passive seismic data. Careful editing of road-generated noise was critical to success. In relatively quiet areas, both PSD-IZ and TRI-E attributes provide similar results. In high-noise areas near a large export pipeline, TRI-E partially mitigated this noise by suppressing surface waves, resulting in more interpretable profiles.

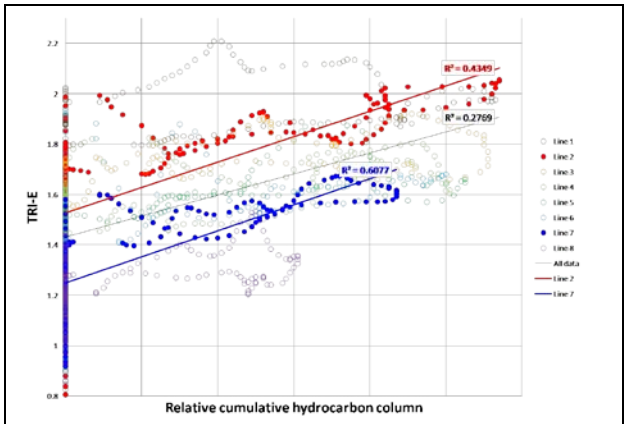

Figure 9: TRI-E vs. relative cumulative hydrocarbon column for all Shaheen lines. Lines 2 and 7 are highlighted. Slopes of the correlations are similar but are offset due to the pipeline noise.

Attribute maps and profiles at Shaheen show that low energy attribute areas are low potential. This allows us to focus on the higher potential areas. Comparisons to reservoir fluid data are preliminary as presented, but encouraging. We see similar slopes in the correlation of LF seismic attributes to a hydrocarbon thickness measure along lines of acquisition. Acquisition and processing schemes will need to improve to make this a quantitative reservoir characterization tool in the face of severe oil field noise.

Observations of increased LF seismic anomalies over the thick oil reservoir following large teleseismic earthquake events provide additional confirmation that this energy measure is related to a local reservoir process. The map of energy attributes from 2-3 Hz does not correlate to maps of high frequency noise energy, which is centered at infrastructure locations. The 1.9-3 Hz energy attributes correlate somewhat to the surface projection of the reservoir, and potentially scale to net hydrocarbon column thickness from the reservoir.

Acknowledgements

We thank Abu Dhabi National Oil Company (ADNOC) and Abu Dhabi Company for Onshore Oil Operations (ADCO) for authorizing the publication of these results. We also would like to acknowledge Ahmed Khouri, Mahfoud Al Jenaibi, Salem Al Amri, Abdulnaser Abousetta and Hani Nehaid for their support, encouragement and valuable contributions. The array data were collected through cooperation with the Petroleum Institute of Abu-Dhabi, thanks to K. Berteussen and M. Ali. Some results were produced using the Sesarray package (www.geopsy.org, e.g. Wathelet *et al.*, 2008).

EDITED REFERENCES

Note: This reference list is a copy-edited version of the reference list submitted by the author. Reference lists for the 2010 SEG Technical Program Expanded Abstracts have been copy edited so that references provided with the online metadata for each paper will achieve a high degree of linking to cited sources that appear on the Web.

REFERENCES

Ali, M., K. Berteussen, J. Small, and B. Barkat, 2010, A study of ambient noise over an onshore oil field in Abu Dhabi, United Arab Emirates: Bulletin of the Seismological Society of America, **100**, no. 1, 392–401, doi:10.1785/0120090131.

Artman, B., I. Podlachikov, and A. Goertz, 2009, Elastic time-reverse modeling imaging conditions: 79th Annual International Meeting, SEG, Expanded Abstracts, 1207–1211.

Dangel, S., M. E. Schaepman, E. P. Stoll, R. Carniel, O. Barzandji, E.-D. Rode, and J. M. Singer, 2003, Phenomenology of tremor-like signals observed over hydrocarbon reservoirs: Journal of Volcanology and Geothermal Research, **128**, no. 1-3, 135–158, doi:10.1016/S0377-0273(03)00251-8.

Lambert, M.-A., S. M. Schmalholz, E. H. Saenger, and B. Steiner, 2009, Low-frequency microtremor anomalies at an oil and gas field in Voitsdorf, Austria: Geophysical Prospecting, **57**, no. 3, 393–411, doi:10.1111/j.1365-2478.2008.00734.x.

Saenger, E. H., S. Schmalholz, M.-A. Lambert, T. T. Nguyen, A. Torres, S. Metzger, R. Habiger, T. Müller, S. Rentsch, and E. Méndez-Hernández, 2009, A passive seismic survey over a gas field: Analysis of low-frequency anomalies: Geophysics, 74, no. 2, O29–O40, doi:10.1190/1.3078402.

Saenger, E. H., 2000: Wave propagation in fractured media: Theory and applications of the rotated staggered grid, PhD thesis, Karlsruhe University.

Witten, B., and B. Artman, 2010, Signal to noise estimates of time-reverse images: EAGE Extended Abstracts.

Wathelet, M., D. Jongmans, M. Ohrnberger, and S. Bonnefoy-Claudet, 2008, Array performances for ambient vibrations on a shallow structure and consequences over Vs inversion: Journal of Seismology, **12**, no. 1, 1–19, doi:10.1007/s10950-007-9067-x.